DESY 96–205
FSU-HEP-960917
CERN-TH/96-262
September 1996

The Heavy-Flavour Contribution to Proton Structure

K. Daum

Rechenzentrum, Universität Wuppertal
Gaußstraße 20, D-42097 Wuppertal, Germany

S. Riemersma

DESY–Zeuthen
Platanenallee 6, D–15735 Zeuthen, Germany

B.W. Harris

Department of Physics, Florida State University
Tallahassee, Florida, 32306-3016, USA

E. Laenen

CERN Theory Division
CH-1211 Geneva 23, Switzerland

J. Smith

Institute for Theoretical Physics, SUNY Stony Brook
Stony Brook NY 11794-3840, USA

Abstract

We present theoretical and experimental considerations pertaining to deeply inelastic heavy-flavour production at HERA. The various theoretical uncertainties in the cross section calculation are discussed. Cuts are imposed to determine the fraction of charm production accessible to the detectors. The production of charm at asymptotic Q^2 and bottom production are also covered. Experimental aspects include current charm production data analysis and prospects for future analyses including anticipated high precision and distinguishing photon-gluon fusion charm events from excitation from the charm parton density. The feasibility of measuring $F_2^{b\bar{b}}(x, Q^2)$ is investigated.

* *To appear in abbreviated form in the proceedings of the workshop "Future Physics at HERA", DESY, Hamburg, 1996.*

The Heavy-Flavour Contribution to Proton Structure

K. Daum[a,b], S. Riemersma[c], B.W. Harris[d], E. Laenen[e], J. Smith[b,f]

[a] Rechenzentrum, Universität Wuppertal, Gaußstraße 20, D-42097 Wuppertal, Germany
[b] DESY, Notkestrasse 85, D-22603 Hamburg, Germany
[c] DESY-Zeuthen, Platanenallee 6 D-15738 Zeuthen, Germany
[d] Department of Physics, Florida State University, Tallahassee, Florida, 32306-3016, USA
[e] CERN Theory Division, CH-1211 Geneva 23, Switzerland
[f] Institute for Theoretical Physics, SUNY Stony Brook, NY 11794-3840, USA

Abstract: We present theoretical and experimental considerations pertaining to deeply inelastic heavy-flavour production. The various theoretical uncertainties in the cross section calculation are discussed. Cuts are imposed to determine the fraction of charm production accessible to the detectors. The production of charm at asymptotic Q^2 and bottom production are also covered. Experimental aspects include current charm production data analysis and prospects for future analyses including anticipated high precision and distinguishing photon-gluon fusion charm events from excitation from the charm parton density. The feasibility of measuring $F_2^{b\overline{b}}(x,Q^2)$ is investigated.

1 Introduction

Heavy-flavour production in deeply inelastic scattering (DIS) at HERA is now emerging as a very important means of studying proton structure. The ink is still drying on the first experimental reports of charm production from photon-mediated DIS at HERA [1, 2]. The next-to-leading order (NLO) calculations have also been published within the last four years. The inclusive calculation of the photon-mediated heavy-flavour structure functions $F_{2,L}^{\rm hq}(x,Q^2,m^2)$ [3], the inclusive single differential distribution $dF_{2,L}^{\rm hq}/dO$ [4] (O being the transverse momentum p_t of the heavy quark and the rapidity y), and the fully differential calculation [5] are now available for a complete NLO analysis of the photon-mediated heavy-flavour structure function.

In section 2, following a short review of the necessary formulae, we investigate various theoretical issues surrounding DIS heavy-flavour production. The primary sources of theoretical uncertainty include the imprecisely determined charm quark mass and renormalization and factorization scale dependences. Additional impediments to a clean extraction of the gluon density from heavy-flavour production include the effects of light-quark (u,d,s) initiated heavy-flavour production and the influence of the longitudinal heavy-flavour structure function $F_L^{\rm hq}(x,Q^2,m^2)$ upon the cross section results.

We investigate the effect of realistic cuts in p_t and pseudorapidity η on the cross section and determine acceptance probabilities as a function of x and Q^2. Charm production in the

limit $Q^2 \gg m_c^2$ [6] and the transition of charm production from boson-gluon fusion at low Q^2 to excitation from the charm density as Q^2 becomes much larger than m_c^2 is then discussed, followed by a cursory view of bottom production.

In section 3, we discuss the analysis of the 1994 HERA data. Identification methods of the produced $D^0, D^{*\pm}$ are outlined. The measured cross section [1] is compared with various theoretical predictions. A determination of the source of the charm production is performed, revealing the primary production mechanism at presently measured Q^2 values is photon-gluon fusion rather than stemming from the charm parton density. The charm structure function $F_2^{c\overline{c}}$ is extracted and the ratio $F_2^{c\overline{c}}/F_2$ is determined.

Future experimental prospects include the installation of silicon vertex detectors, enabling greater charm and bottom hadron detection efficiency. The anticipated luminosity of $500\,pb^{-1}$ will allow detailed studies of charm production dynamics. The transition from boson-gluon fusion of charm to excitation from the charm quark sea should become apparent as the accessible Q^2 grows. The predicted bottom quark production cross section will enable studies of $F_2^{b\overline{b}}/F_2^{c\overline{c}}$ as a function of x and Q^2 with reasonable precision.

2 Theoretical Aspects

2.1 Background

The reaction under study is

$$e^-(l) + P(p) \rightarrow e^-(l') + Q(p_1)(\bar{Q}(p_1)) + X\,, \tag{1}$$

where $P(p)$ is a proton with momentum p, $Q(p_1)(\bar{Q}(p_1))$ is a heavy (anti)-quark with momentum p_1 ($p_1^2 = m^2$) and X is any hadronic state allowed by quantum number conservation. The cross section may be expressed as

$$\frac{d^2\sigma}{dx\,dQ^2} = \frac{2\pi\alpha^2}{x\,Q^4}\left[(1+(1-y)^2)F_2^{\rm hq}(x,Q^2,m^2) - y^2 F_L^{\rm hq}(x,Q^2,m^2)\right]\,, \tag{2}$$

where

$$q = l - l'\,, \qquad Q^2 = -q^2\,, \qquad x = \frac{Q^2}{2p\cdot q}\,, \qquad y = \frac{p\cdot q}{p\cdot l}\,. \tag{3}$$

The inclusive structure functions $F_{2,L}^{\rm hq}$ were calculated to next-to-leading order (NLO) in Ref. [3]. The results can be written as

$$\begin{aligned} F_k(x,Q^2,m^2) &= \frac{Q^2\alpha_s(\mu^2)}{4\pi^2 m^2}\int_x^{z_{\rm max}}\frac{dz}{z}\left[\,e_H^2 f_g(\frac{x}{z},\mu^2)c_{k,g}^{(0)}\,\right] \\ &+ \frac{Q^2\alpha_s^2(\mu^2)}{\pi m^2}\int_x^{z_{\rm max}}\frac{dz}{z}\Big\{\,e_H^2 f_g(\frac{x}{z},\mu^2)(c_{k,g}^{(1)} + \bar{c}_{k,g}^{(1)}\ln\frac{\mu^2}{m^2}) \\ &+ \sum_{i=q,\bar{q}}\left[e_H^2\, f_i(\frac{x}{z},\mu^2)(c_{k,i}^{(1)} + \bar{c}_{k,i}^{(1)}\ln\frac{\mu^2}{m^2}) + e_{L,i}^2\, f_i(\frac{x}{z},\mu^2)d_{k,i}^{(1)}\,\right]\Big\}\,, \end{aligned} \tag{4}$$

where $k = 2, L$ and the upper boundary on the integration is given by $z_{\rm max} = Q^2/(Q^2+4m^2)$. The functions $f_i(x,\mu^2)\,,(i = g,q,\bar{q})$ denote the parton densities in the proton and μ stands

for the mass factorization scale which has been set equal to the renormalization scale. The $c_{k,i}^{(l)}(\zeta,\xi)\,(i = g\,,q\,,\bar{q}\,;l = 0,1)$, $\bar{c}_{k,i}^{(l)}(\zeta,\xi)\,(i = g,q,\bar{q};l = 1)$, and $d_{k,i}^{(l)}(\zeta,\xi)\,(i = q\,,\bar{q}\,;l = 1)$ are coefficient functions and are represented in the $\overline{\rm MS}$ scheme. They depend on the scaling variables ζ and ξ defined by

$$\zeta = \frac{s}{4m^2} - 1 \qquad \xi = \frac{Q^2}{m^2}\,. \tag{5}$$

where s is the square of the c.m. energy of the virtual photon-parton subprocess $Q^2(1-z)/z$. In Eq. (4) we distinguish between the coefficient functions with respect to their origin. The coefficient functions indicated by $c_{k,i}^{(l)}(\zeta,\xi), \bar{c}_{k,i}^{(l)}(\zeta,\xi)$ originate from the partonic subprocesses where the virtual photon is coupled to the heavy quark, whereas $d_{k,i}^{(l)}(\zeta,\xi)$ comes from the subprocess where the virtual photon interacts with the light quark. The former are multiplied by the charge squared of the heavy quark e_H^2, and the latter by the charge squared of the light quark e_L^2 respectively (both in units of e). Terms proportional to $e_H e_L$ integrate to zero for the inclusive structure functions. Furthermore we have isolated the factorization scale dependent logarithm $\ln(\mu^2/m^2)$.

The scale dependence and the poorly known charm quark mass are the largest contributors to the theoretical uncertainty. The effects of $F_L^{\rm hq}$ and the light-quark initiated contributions are discovered also to be important in the analysis. To aid the experimental analysis, the fully differential program [5] is used to apply a series of cuts to determine the percentage of events the detectors are likely to see in bins of x and Q^2. With the planned inclusion of silicon vertex detectors, the ability to see bottom events increases dramatically, motivating the presentation of results for the cross section and $F_2^{b\bar{b}}(x,Q^2,m_b^2)$. HERA is in a unique position to evaluate the transition of charm production from photon-gluon fusion to excitation from the charm parton density. For other phenomenological investigations, see [8, 9, 10].

2.2 Code Update

For this study we use an updated version of the code based upon [7]. The original code was based upon fitting the coefficient functions described in eq. (4) using a two-dimensional tabular array of points in ζ and ξ. The coefficient functions were generated via a linear interpolation between the calculated points. The linear interpolation was insufficiently accurate and required a more sophisticated interpolation procedure.

The present interpolation procedure is based upon a Lagrange three-point interpolation formula, see eq. 25.2.11 [11]. The results have been thoroughly compared with the original code in [3] and [5] and excellent agreement has been established.[1]

As a demonstration of the code, we present results for the Born $c_2^{(0)}(\zeta,\xi = 1,10)$ in Fig. 1 and $c_{2,g}^{(1)}(\zeta,\xi = 1,10)$ and $\overline{c}_{2,g}^{(1)}(\zeta,\xi = 1,10)$ in Fig. 2.

2.3 Scale and Parton Density Related Issues

The most important numerical sources of theoretical uncertainty in DIS heavy-flavour production are the factorization/renormalization scale dependence and the poorly known charm quark

[1] The code is available at http://www.ifh.de/theory/publist.html.

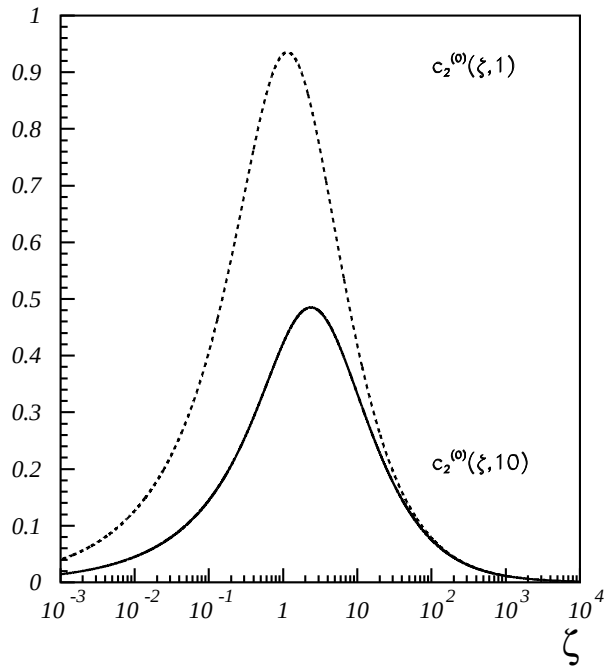

Figure 1: *The Born coefficient function* $c_2^{(0)}(\zeta,\xi)$*, for* $\xi = 1, 10$.

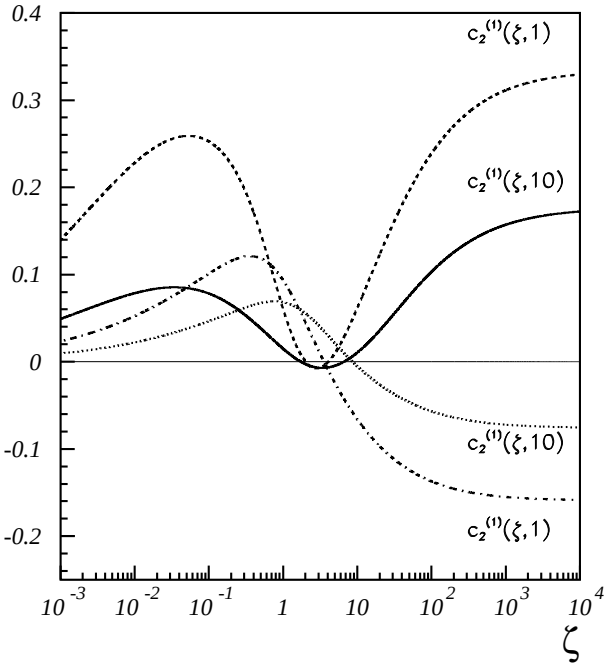

Figure 2: *The NLO coefficient functions* $c_{2,g}^{(1)}(\zeta,\xi)$*, for* $\xi = 1, 10$ *(upper curves at large* ζ*) and* $\overline{c}_{2,g}^{(1)}(\zeta,\xi)$ *for* $\xi = 1, 10$ *(lower curves at large* ζ*).*

mass. Varying μ in Eq. (4) indicates the stability of the NLO result against scale changes. To get a concrete idea of the effect of scale variations, we first construct a "data" set. The number of DIS charm events is calculated for an integrated luminosity of $500\,pb^{-1}$, using CTEQ3M [12] parton densities with $\Lambda_4 = 239$ MeV, $m_c = 1.5$ GeV, and $\mu^2 = Q^2 + 4\,m_c^2$. Unless otherwise mentioned, CTEQ3M is used for all results. The results in Fig. 3. are produced for $1.8 < Q^2 < 1000$ GeV^2 and $10^{-4} < x < 1$ using four bins per decade for both Q^2 and x. The

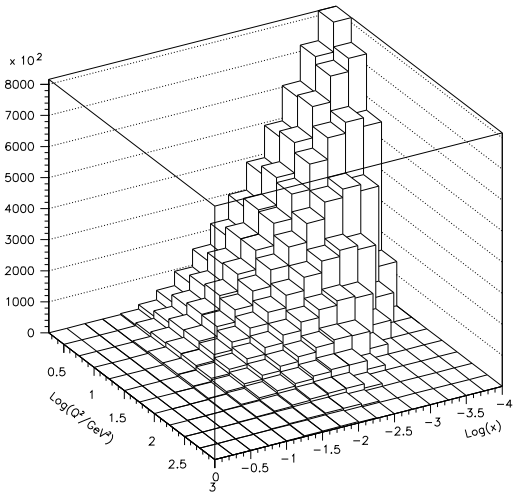

Figure 3: *Projected number of DIS charm events for an integrated luminosity of 500 pb^{-1} binned in x and Q^2 with no cuts applied.*

"data" are peaked strongly at small x and Q^2. As Q^2 grows, the events become more evenly distributed in x. For small Q^2, the number of events N falls off as $x \to 1$. At larger Q^2, N rises, peaks at intermediate x, then drops.

Using the "data" set as a point of reference, we can investigate where in the kinematic region the effects of scale variation are most strongly felt. Keeping every other parameter fixed, we determine the number of events for $\mu^2 = 4m_c^2$ and $\mu^2 = 4(Q^2 + 4m_c^2)$. We investigate the quantity

$$\Delta_\mu(x, Q^2) \equiv \left| \frac{N(\mu^2 = 4m_c^2) - N(\mu^2 = 4(Q^2 + 4m_c^2))}{2N(\mu^2 = Q^2 + 4m_c^2)} \right|. \tag{6}$$

The results are displayed in Fig.. 4. Apart from the high-x region, which contains very few charm events, the scale dependence varies relatively little with Q^2. As $x \to 0$, we find the scale dependence disappearing. This behaviour bodes very well for a low-x extraction of the gluon density from charm events.

The charm quark mass uncertainty presents a stickier problem. A precise measurement of the charm mass is yet to be made. To develop a feeling for how much of an effect the uncertainty has, we calculated

$$\Delta_{m_c}(x, Q^2) \equiv \frac{N(m_c = 1.3\text{GeV}) - N(m_c = 1.7\text{GeV})}{2\,N(m_c = 1.5\text{GeV})}. \tag{7}$$

Very large effects are naturally found near threshold, but as Q^2 increases and x decreases, Δ_{m_c} approaches a value on the order of 0.1. Varying the charm mass from 1.3 to 1.7 GeV is a

conservative estimate; the error induced by the uncertainty viewed in Fig. 5. can be viewed as an upper bound.

A clear indication of the ability to extract the gluon density from charm production is whether one can distinguish the gluon densities from different available parton densities. We compare the cross section generated with CTEQ2MF[12] (with a flat gluon density as $x \to 0$) with GRV94HO[13] (with a steep gluon density as $x \to 0$). We define

$$\Delta_{\rm glue}(x, Q^2) \equiv \left| \frac{N_{\rm CTEQ2MF} - N_{\rm GRV94HO}}{2\, N_{\rm CTEQ3M}} \right| \tag{8}$$

and show the results in Fig. 6. Away from large x, $\Delta_{\rm glue}(x, Q^2)$ is flat as a function of Q^2. In the intermediate region in x, very little distinguishing power is observed. Beginning near $x = 10^{-3}$, a definite difference is seen. The analysis must seemingly extend to $x \lesssim 5 \cdot 10^{-4}$ to distinguish cleanly the gluon densities mentioned.

To summarize: While the scale dependence is well under control, the dominant source of uncertainty is clearly the charm quark mass, which has a strong influence on the cross section at low x and low Q^2. This region is exactly the region sensitive to the gluon density. This strong influence of m_c poses problems for a clean extraction of the gluon density at small x from inclusive measurements.

2.4 Smaller Contributions to the Cross Section: $F_L^{c\bar{c}}$ and Light-Quark Initiated Results

A clean extraction of the gluon density may be hindered by contributions of $F_L^{c\bar{c}}$ and light-quark initiated contributions to the cross section. We investigate the fractional F_L contribution to the cross section by plotting

$$C_{F_L} \equiv \left| \frac{\sigma_{tot} - \sigma_{F_2}}{\sigma_{tot}} \right|, \tag{9}$$

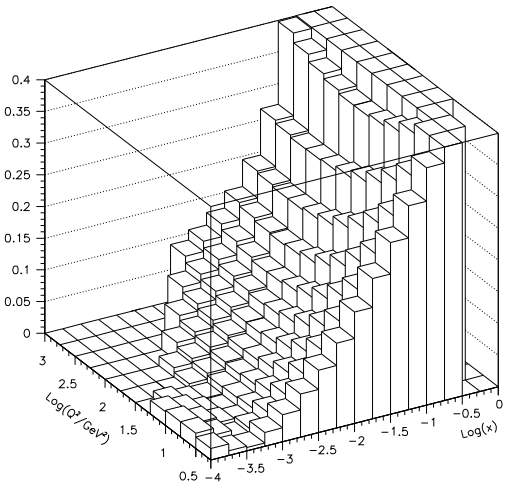

Figure 4: $\Delta_\mu(x, Q^2)$ *(see Eq. (6)) binned in* x *and* Q^2.

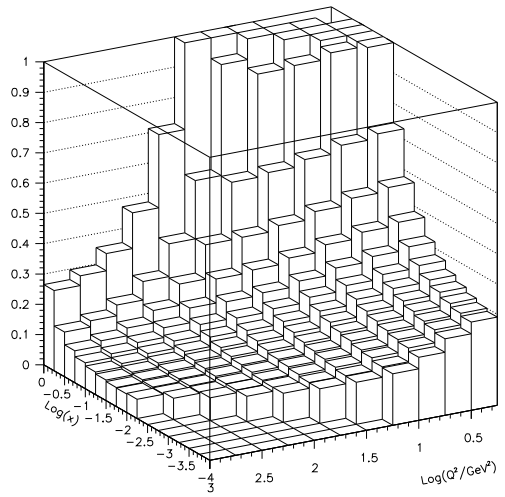

Figure 5: $\Delta_{m_c}(x, Q^2)$ *(see Eq. (7)) binned in* x *and* Q^2*.*

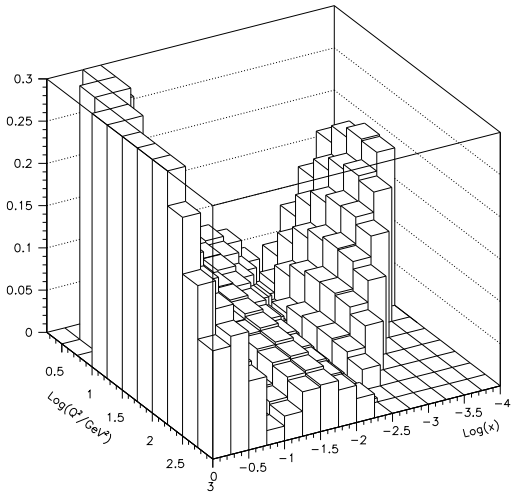

Figure 6: $\Delta_{\rm glue}(x, Q^2)$ *(see Eq. (8)) binned in* x *and* Q^2*.*

where σ_{F_2} represents the contribution to the cross section in Eq. (2) with F_L set to zero. The results are shown in Fig. 7. We find a sizeable contribution to the cross section at high y. This overlaps with the low Q^2 and low x region previously determined to be deemed the most suitable for a gluon density extraction. To do so, however, one must take into consideration $F_L^{c\overline{c}}$.

We investigate the light-quark initiated contribution by determining

$$C_{\rm lq} = \left| \frac{\sigma_{\rm lq}}{\sigma_{tot}} \right| \tag{10}$$

and displaying the results in Fig. 8. The results are very nearly constant, amounting to a 5 – 8 % contribution except at large x, where the charm contribution does not appreciably contribute numerically.

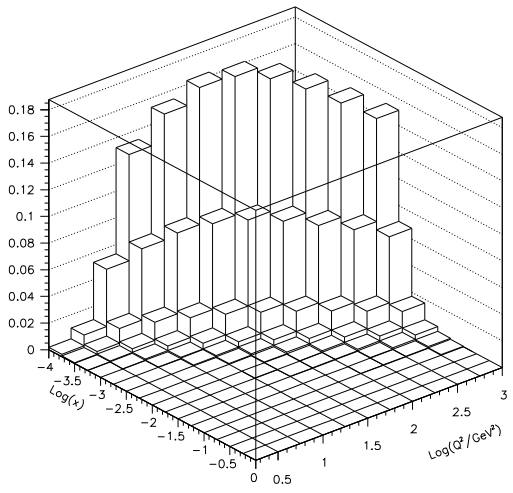

Figure 7: $C_{F_L}(x, Q^2)$ *(see Eq. (9)) binned in* x *and* Q^2*.*

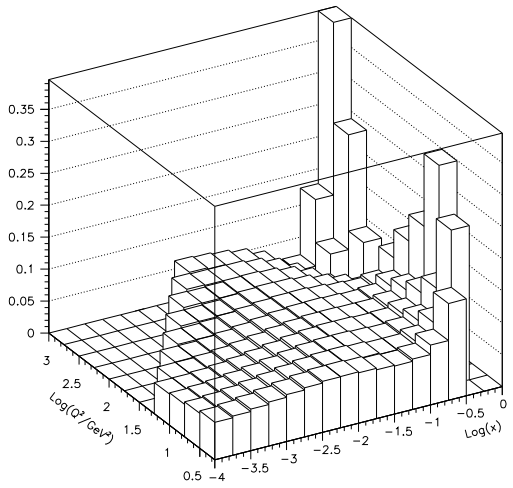

Figure 8: C_{lq} *(see Eq. (10)) binned in* x *and* Q^2*.*

Summarizing: the contributions to the cross section from $F_L^{c\overline{c}}$ are noticeable in the large y region, which overlaps with the small x and small Q^2 region, hindering the extraction of the gluon using only $F_2^{c\overline{c}}$. The light-quark initiated cross section contributes on the order of 5 % to the total cross section, and therefore cannot be totally neglected.

2.5 Cuts *vs.* No Cuts

With the fully differential code developed in [5], a series of cuts can be applied determining a more realistic expectation of charm events able to be detected.

The cuts imposed upon the data are

$$|\eta_c| \leq 1.5,\ p_t^c \geq 2\,\mathrm{GeV}, \tag{11}$$

x_{min}	x_{max}	σ (nb)	σ_{cuts} (nb)	Efficiency (%)
0.1000E-03	0.1778E-03	0.439E+01	0.106E+01	24.1
0.1778E-03	0.3162E-03	0.414E+01	0.113E+01	27.3
0.3162E-03	0.5623E-03	0.360E+01	0.961E+00	26.7
0.5623E-03	0.1000E-02	0.296E+01	0.704E+00	23.8
0.1000E-02	0.1778E-02	0.232E+01	0.396E+00	17.1
0.1778E-02	0.3162E-02	0.174E+01	0.171E+00	9.8
0.3162E-02	0.5623E-02	0.125E+01	0.381E-01	3.0
0.5623E-02	0.1000E-01	0.853E+00	0.189E-02	0.22

Table 1: *Cross sections with and without the cuts mentioned in Eq. (11) for* $2 < Q^2 < 10$ GeV^2.

x_{min}	x_{max}	σ (nb)	σ_{cuts} (nb)	Efficiency (%)
0.1000E-03	0.1778E-03	0.334E+00	0.584E-01	17.5
0.1778E-03	0.3162E-03	0.116E+01	0.251E+00	21.6
0.3162E-03	0.5623E-03	0.173E+01	0.484E+00	28.0
0.5623E-03	0.1000E-02	0.198E+01	0.681E+00	34.4
0.1000E-02	0.1778E-02	0.191E+01	0.768E+00	40.2
0.1778E-02	0.3162E-02	0.162E+01	0.701E+00	43.3
0.3162E-02	0.5623E-02	0.127E+01	0.504E+00	39.7
0.5623E-02	0.1000E-01	0.945E+00	0.280E+00	29.6
0.1000E-01	0.1778E-01	0.660E+00	0.112E+00	17.0
0.1778E-01	0.3162E-01	0.430E+00	0.254E-01	5.9
0.3162E-01	0.5623E-01	0.256E+00	0.136E-02	5.3
0.5623E-01	0.1000E+00	0.131E+00	0.468E-05	0.0036

Table 2: *Cross sections with and without the cuts mentioned in Eq. (11) for* $10 < Q^2 < 100$ GeV^2.

η_c being the pseudorapidity of the detected charm quark. Looking first at the low Q^2 range from 2 to 10 GeV^2, we present the cross section with and without the aforementioned cuts in the x bins outlined in Tab. 1. These results were generated using GRV94HO, $m_c = 1.5$ GeV, 3 light flavours, and $\Lambda_3 = 248$ MeV. In the low x range, we observe an efficiency of 20 – 25 %, diminishing near threshold, the low efficiency mostly a result of the p_t cut.

Table 2 displays results in the medium Q^2 range, from 10 to 100 GeV^2. We find the efficiency has risen considerably to the 30–40 % range where the cross section is peaked in intermediate x, with on the order of 20 % for the small x region.

In the large Q^2 range, from 100 to 1000 GeV^2, the results are found in Tab. 3. The efficiency continues to rise with Q^2, reaching 50–60 % in the high to intermediate x region and 30–40 % in the small x range.

The number of events landing within the imposed cuts mentioned in Eq. (11) is not overwhelmingly large, but a large enough sample should be accessible to gather significant statistics.

x_{min}	x_{max}	σ (nb)	σ_{cuts} (nb)	Efficiency (%)
0.1000E-02	0.1778E-02	0.401E-01	0.120E-01	29.9
0.1778E-02	0.3162E-02	0.124E+00	0.486E-01	39.2
0.3162E-02	0.5623E-02	0.159E+00	0.885E-01	55.7
0.5623E-02	0.1000E-01	0.157E+00	0.958E-01	61.0
0.1000E-01	0.1778E-01	0.128E+00	0.757E-01	59.1
0.1778E-01	0.3162E-01	0.906E-01	0.458E-01	50.6
0.3162E-01	0.5623E-01	0.572E-01	0.173E-01	30.2
0.5623E-01	0.1000E+00	0.315E-01	0.285E-02	9.1
0.1000E+00	0.1778E+00	0.140E-01	0.167E-03	1.2
0.1778E+00	0.3162E+00	0.407E-02	0.400E-05	0.098
0.3162E+00	0.5623E+00	0.466E-03	0.413E-08	0.0009

Table 3: *Cross sections with and without the cuts mentioned in Eq. (11) for* $100 < Q^2 < 1000$ GeV^2.

2.6 Charm Production at Asymptotic Q^2

Near the threshold for charm production the deep inelastic structure functions F_i, $i = 2, L$, which include the contributions of the light partons u, d, s, and g and the charm quark with mass m_c are given by

$$\begin{aligned} F_i(Q^2, m_c^2, 3) = \frac{2}{9}\Big[\Sigma(\mu^2,3) \otimes \Big\{C_{i,q}^{\rm S}\Big(\frac{Q^2}{\mu^2}, 3\Big) + L_{i,q}^{\rm S}\Big(\frac{Q^2}{m_c^2}, \frac{m_c^2}{\mu^2}, 3\Big)\Big\}\Big] \\ + G(\mu^2,3) \otimes \Big\{C_{i,g}^{\rm S}\Big(\frac{Q^2}{\mu^2}, 3\Big) + L_{i,g}^{\rm S}\Big(\frac{Q^2}{m_c^2}, \frac{m_c^2}{\mu^2}, 3\Big)\Big\} \\ + \Delta(\mu^2,3) \otimes \Big\{C_{i,q}^{\rm NS}\Big(\frac{Q^2}{\mu^2}, 3\Big) + L_{i,q}^{\rm NS}\Big(\frac{Q^2}{m_c^2}, \frac{m_c^2}{\mu^2}, 3\Big)\Big\} \\ + \frac{4}{9}\Big[\Sigma(\mu^2,3) \otimes H_{i,q}^{\rm PS}\Big(\frac{Q^2}{m_c^2}, \frac{m_c^2}{\mu^2}, 3\Big) \\ + G(\mu^2,3) \otimes H_{i,g}^{\rm S}\Big(\frac{Q^2}{m_c^2}, \frac{m_c^2}{\mu^2}, 3\Big)\Big], \end{aligned} \tag{12}$$

where we have the following definitions. The variable Q^2 denotes the virtual mass squared of the photon exchanged between the electron and the proton.. The momenta of the photon and the proton are given by q and p respectively and the Bjorken scaling variable is defined by $x = Q^2/(2p \cdot q)$ ($q^2 = -Q^2 < 0$). The structure functions F_i depend on x, on Q^2 and on the charm quark mass m_c. The convolution symbol $\otimes$ appears on the right-hand-side which is defined by

$$(f \otimes g)(x) = \int_0^1 dz_1 \int_0^1 dz_2\, \delta(x - z_1 z_2)\, f(z_1)\, g(z_2)\,. \tag{13}$$

The gluon density is denoted by $G(\mu^2, 3)$ where the number of light flavours n_f is taken to be three. Also the singlet and nonsinglet combinations of the light quark densities are defined for $n_f = 3$ as follows

$$\begin{aligned} \Sigma(\mu^2,3) = u(\mu^2,3) + \bar{u}(\mu^2,3) + d(\mu^2,3) + \bar{d}(\mu^2,3) \\ + s(\mu^2,3) + \bar{s}(\mu^2,3)\,, \end{aligned} \tag{14}$$

$$\Delta(\mu^2,3) = \frac{2}{9}\Big[u(\mu^2,3)+\bar{u}(\mu^2,3)\Big] - \frac{1}{9}\Big[d(\mu^2,3)+\bar{d}(\mu^2,3) + s(\mu^2,3)+\bar{s}(\mu^2,3)\Big]\,. \tag{15}$$

The same singlet and non-singlet classification can also be made for the light parton coefficient functions $C_{i,k}$ ($i = 2, L, k = q, g$) and the heavy quark coefficient functions $L_{i,k}$, $H_{i,k}$, $H_{i,k}$ depending on m_c. The coefficient functions $L_{i,k}$, $H_{i,k}$ reflect the corresponding production processes. The functions $H_{i,k}$ contain the processes where the virtual photon couples to the heavy quark (*c.f.* Figs. 2, 3, 4, 5.a and 5.b in [3]), whereas $L_{i,k}$ describe the reactions where the virtual photon couples to the light quark (*c.f.* Figs. 5.c and 5.d in [3]). Hence $L_{i,k}$ and $H_{i,k}$ are multiplied by e_i^2 (where $1/n_f \sum_{i=1}^{3} e_i^2 = 2/9$) and by e_c^2 (where $e_c = 2/3$) respectively. These charge factors are exhibited by Eq. (12). Furthermore both the coefficient functions and the parton densities depend on the mass factorization scale μ, which, for convenience will be set equal to the renormalization scale. The latter also shows up in the running coupling constant $\alpha_s(\mu^2, 3)$ where the number of light flavours is three.

Equation (12) gives an adequate prescription as long as the c.m. energy is not too far above the charm threshold, which implies that Q^2 is not too large compared to m_c^2. However, when we enter the asymptotic region $Q^2 \gg m_c^2$, the heavy quark coefficient functions behave like $\ln^i(m_c^2/\mu^2)\ln^j(Q^2/m_c^2)$ so that the higher order corrections can become large. At sufficiently large Q^2 the charm quark should be treated in the same way as the light partons were at smaller Q^2. The logarithmic behaviour of the coefficient functions is due to the collinear singularities which are regulated by m_c. Therefore when $Q^2 \gg m_c^2$, the charm quark behaves like a massless quark similar to the behaviour of the normal light quarks (u, d, and s) over the whole Q^2 range. Following the same procedure as has been used for the light partons, the mass singular (m_c -dependent) terms have to be factorized out of the heavy quark coefficient functions using the method of mass factorization. This leads to a redefinition of the parton densities in Eqs. (14), (15) and the heavy quark coefficient functions turn into the light parton analogues, wherein the number of light flavours is enhanced by one. The above procedure is called the variable flavour number scheme (VFNS) which is outlined in leading order in [14].

Since all coefficient functions are now available up to order α_s^2, this analysis can be extended to NLO to give a better description for the structure functions $F_i(x, Q^2)$ at large Q^2. A preprint is in preparation[15].

2.7 Bottom Quark Production

The anticipated amount of bottom production is greatly reduced due to the reduction of the charge factor by four as well as a significantly reduced phase space. Given a luminosity of 500 pb^{-1}, however, thousands of events are expected per bin of x and Q^2 as shown in Fig. 9. We take $m_b = 4.75$ GeV, the factorization scale $\mu^2 = Q^2 + m_b^2$, as well as the CTEQ3M distributions. A discussion of the implications of this number of b events can be found in section 3.2.2.

3 Experimental Aspects

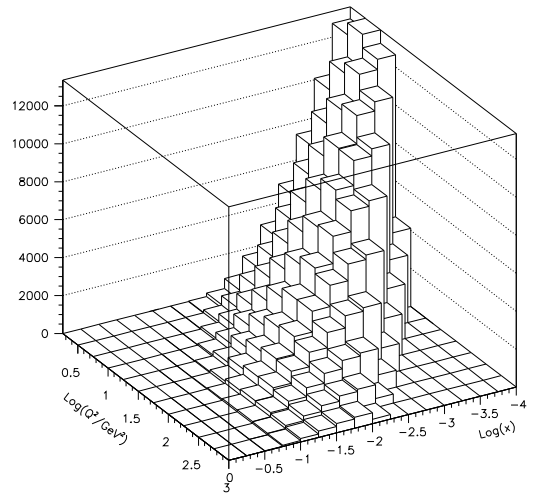

Figure 9: *Projected number of DIS bottom events for an integrated luminosity of 500 pb^{-1} binned in x and Q^2 with no cuts applied.*

3.1 Current Experimental Situation

Results on charm production in deep inelastic ep scattering are available from both experiments H1 and ZEUS based on an integrated luminosity of roughly 3 pb^{-1} collected with each experiment at HERA in 1994. The H1 collaboration [1] has performed the tagging of heavy quark events by reconstructing $D^0(1864)$[2] and $D^{*+}(2010)$ mesons, while the ZEUS collaboration [2] has given preliminary results for the inclusive $D^{*+}(2010)$ analysis.

The D^0 is identified via its decay mode $D^0 \to K^-\pi^+$ and the D^{*+} through the decay chain $D^{*+} \to D^0\pi^+_{slow} \to K^-\pi^+\pi^+_{slow}$. For the latter use is made of the tight kinematic constraint for the decay of $D^{*+} \to D^0\pi^+_{slow}$ [16]. A better resolution is expected for the mass difference $\Delta m = m(D^0\pi^+_{slow}) - m(D^0)$ than for the D^{*+} mass itself.

Figure 10 shows the $m_{K\pi}$ distribution obtained in the inclusive D^0 analysis of H1 and the Δm distribution as observed in the inclusive D^{*+} of ZEUS. Evidently the number of observed events containing heavy quarks is small. Only of the order of 100 to 200 charm mesons are identified in any of the different analyses. Combining the D^0 and $D^{*\pm}$ analysis of H1 leads to a charm production cross section of

$$\sigma(ep \to ec\bar{c}X) = 17.4 \pm 1.6 \pm 1.7 \pm 1.4 \text{ nb} \tag{16}$$

in the kinematic range 10 $\text{GeV}^2 < \text{Q}^2 < 100$ GeV^2 and $0.01 < y < 0.7$. The errors refer to the statistical, the experimental systematic and the model dependent error, respectively. The model dependent error accounts for the uncertainty in the determination of acceptances due to the choice of the parton density in the proton, the mass of the charm quark, and the fragmentation function. This cross section is somewhat larger than predicted by the NLO calculations [3, 1]. The prediction from the gluon density in the proton extracted from the NLO QCD fit of H1 [17] comes closest to the charm data.

[2]Charge conjugate states are always included.

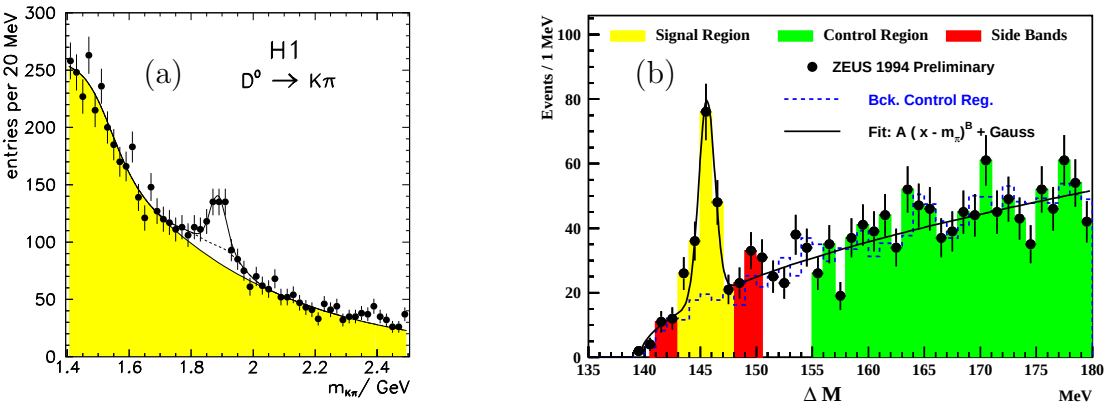

Figure 10: (a) *The $K^-\pi^+$ mass distribution observed in the inclusive D^0 analysis of DIS events from H1, and* (b) *the Δm distribution obtained in the inclusive D^{*+} analysis of DIS events from ZEUS.*

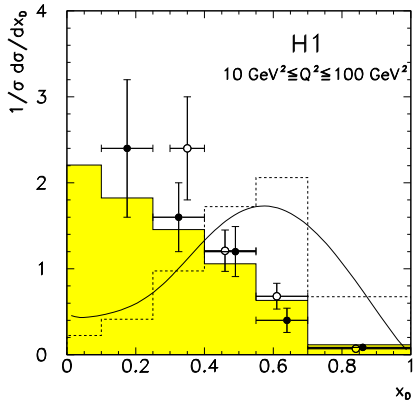

Figure 11: *Normalized x_D distribution in deep inelastic ep scattering at $\langle W \rangle \approx 125$ GeV for $|\eta_D| < 1.5$. The open/closed points represent the D^0/D^* data of H1. The shaded histogram shows the BGF expectation according to AROMA. The dashed histogram shows the charm sea expectation, obtained by selecting QPM events from LEPTO. The full line gives the result of the QCD evolution of the fit to the charged current $\overset{(-)}{\nu}$ N data.*

Information on the charm production mechanism in neutral current DIS at HERA is obtained from the distribution of $x_D = 2|\vec{P}^*_{D^0}|/W$, where $\vec{P}^*_{D^0}$ denotes the momentum of the D^0 in the $\gamma^* p$ system. Figure 11 shows the distributions $1/\sigma \; d\sigma/dx_D$, which are a convolution of the charm production spectrum with the fragmentation function compared to the LO BGF expectation of the AROMA generator. The BGF model agrees very well with the shape of the data. The figure also includes the expectations for charm mesons originating from quarks in the proton either by using LEPTO 6.1 generator [20], from which only charm sea quark events are selected, or by extrapolating the results from charm production in charged current $\overset{(-)}{\nu}$ N scattering [21] to HERA energies. Large differences in the shape of the distributions are observed for the data and these QPM expectations. From these differences, it is concluded that more than 95% of the charm production in neutral current deep inelastic ep scattering is due to boson-gluon fusion. This observation seems to be in contradiction to recent inclusive calculations of charm production in DIS [14], from which was concluded that for the kinematic range accessible in the current analyses at HERA charm quarks may already be considered as partons in the proton [10].

The measurements of the charm contribution $F_2^{c\bar{c}}(x, Q^2)$ to the proton structure function

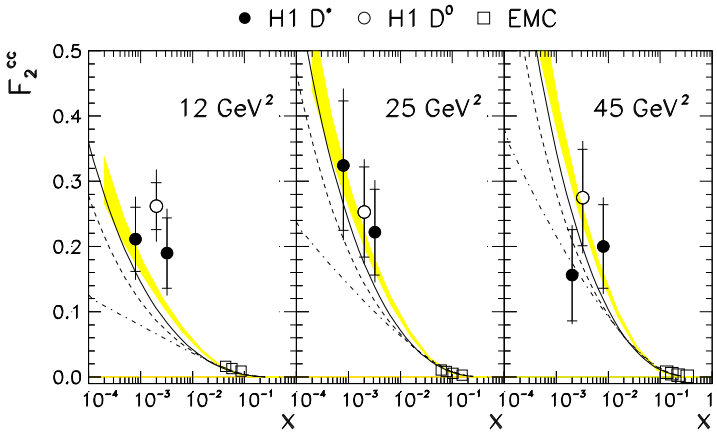

Figure 12: *$F_2^{c\bar{c}}$ as derived from the inclusive D^{*+} (full dots) and D^0 analysis (open circles) in comparison with the NLO calculations based on GRV-HO (full line), MRSH (dashed line), and MRSD0′ (dash-dotted line) parton distributions using a charm quark mass of $m_c = 1.5$ GeV for $\langle Q^2 \rangle = 12,\ 25$ and 45 GeV^2. The inner (outer) error bars refer to the statistical (total) errors. The shaded band represents the prediction from the H1 NLO fit to the F_2 measurements. The EMC data are also shown (open boxes).*

derived from the inclusive D^0 and D^{*+} analysis of H1 are displayed in Fig. 12 together with the results of the EMC collaboration [22] at large x. The measurement at HERA extends the range of the $F_2^{c\bar{c}}$ measurement by two orders of magnitude towards smaller x values. The comparison of the H1 and EMC measurements reveals a steep rise of $F_2^{c\bar{c}}$ with decreasing x. The data are compared with NLO calculations [3] using the GRV-HO [23], the MRSH [24], and the MRSD0′ [25] parameterizations of the gluon density in the proton for a charm quark mass $m_c = 1.5$ GeV. The data are also compared to the prediction from the H1 QCD fit to the F_2 measurements using a charm quark mass of $m_c = 1.5$ GeV. The error band shown for this fit includes the propagation of the statistical and the uncorrelated systematic errors on the total F_2 data through the fitting procedure. This prediction lies systematically above all other calculations, independently of x and Q^2 but agrees better with the $F_2^{c\bar{c}}$ measurement. Within the errors the ratio of $\left\langle F_2^{c\bar{c}}/F_2 \right\rangle$ is found to be independent of x and Q^2. Averaged over the kinematic range a ratio $\left\langle F_2^{c\bar{c}}/F_2 \right\rangle = 0.237 \pm 0.021 \pm 0.041$ is obtained, which is one order of magnitude larger than at larger x measured by EMC.

3.2 Future

3.2.1 Charm Production

In this section some estimates about the precision that may be expected at HERA for an integrated luminosity of 500 pb^{-1} are given. As an example the capabilities of the H1 detector [26] are considered. For heavy flavor physics an important new feature of the apparatus is the double layer silicon vertex detector (CST) [27] which will allow use of the apparent proper time of charm hadrons in selecting heavy flavor events.. Other decay channels than $D^0 \to K^-\pi^+$ and $D^{*+} \to D^0\pi^+_{slow} \to K^-\pi^+\pi^+_{slow}$ are already under investigation or will become accessible due to the CST.

Table 4 contains a list of decay modes which should be feasible for charm tagging in H1 in future by also including the CST. A total charm selection efficiency of 1% may be obtained.

Mode		$P(c \to D)$	$BR(D \to FS)$	ϵ_{tot}	$P \cdot BR \cdot \epsilon_{tot}$
$D^{*+} \to D^0\pi_s^+ \to K^-\pi^+\pi_s^+$	[1]	0.248	0.026	0.16	0.0010
$D^{*+} \to D^0\pi_s^+ \to K^-\pi^+\pi^0\pi_s^+$			0.096	0.04	0.0010
$D^{*+} \to D^0\pi_s^+ \to K^-3\pi\pi_s^+$			0.052	0.10	0.0013
$D^{*+} \to D^0\pi_s^+ \to K^0\pi^+\pi^-\pi_s^+$			0.013	0.20	0.0007
$D^{*+} \to D^0\pi_s^+ \to K^0\pi^+\pi^-\pi^0\pi_s^+$			0.024	0.08	0.0005
$D^{*+} \to D^0\pi_s^+ \to K^-\mu^+\nu_\mu\pi_s^+$			0.024	0.04	0.0002
$D^{*+} \to D^0\pi_s^+ \to K^-e^+\nu_e\pi_s^+$			0.024	0.04	0.0002
Sum D^{*+}		0.248	0.259		0.0049
$D^0 \to K^-\pi^+$	[1]	0.535	0.0383	0.06	0.0012
$D^0 \to K^0\pi^+\pi^-$			0.0186	0.06	0.0006
$D^0 \to K^-3\pi$	CST		0.075	0.04	0.0014
Sum D^0		0.535	0.132		0.0032
$D^+ \to K^0\pi^+$	CST	0.25	0.009	0.12	0.0003
$D^+ \to K^-\pi^+\pi^-$	CST		0.091	0.07	0.0016
$D^+ \to K^03\pi$	CST		0.07	0.07	0.0012
Sum D^+	CST	0.25	0.170		0.0031
Sum D					0.0097

Table 4: *Compilation of various decay channels of charm mesons accessible in H1. The channels marked by "CST" will be accessible only by using the silicon vertex detector. $BR(D \to FS)$ denotes the product of all branching ratios involved in the decay into the final state "FS". For the determination of the total charm tagging efficiency the correlations in the D^0 and D^{*+} analyses are taken into account.*

Compared to the present analysis this corresponds to an increase in the total selection efficiency of a factor 4 to 5. Although the new channels opened by the use of the CST corresponds only to 50% of this gain, the signal to background ratio will improve for all decay modes considerably. Because of this the effective number of events per luminosity $N_{eff} = (N_{signal}/\sigma_{stat})^2$ will increase by a factor of 6 to 8. Due to the cut in the impact parameter of the D^0 mesons, which is likely to be different in the D^0 and D^{*+} analyses, the events selected in the D^{*+} analyses will only partially overlap with the events selected in the corresponding D^0 analyses. Taking an integrated luminosity of 500 pb^{-1} about 160,000 tagged charm events are expected for the kinematic range of the published H1 analysis. This has to be compared to the currently analyzed 250 events. Taking into account the increase in the effective number of events a gain of a factor of 1000 is expected for the statistical significance. In total we expect to observe roughly 6,000 double tag charm events in the range 1.7 GeV$^2 < Q^2 <$ 560 GeV^2 which would allow a study of the charm production dynamics in detail (see Ref. [10]).

Figure 13 shows the result of the hypothetical measurement of $F_2^{c\bar{c}}$ in the range 1.7 GeV$^2 <$ $Q^2 <$ 560 GeV^2 for a luminosity of 500 pb^{-1} based on the gluon density determination from the NLO H1 fit to the inclusive F_2 data combining the statistics of the D meson decay modes summarized in Table 4 by assuming $m_c = 1.5$ GeV and $\mu^2 = Q^2 + 4m_c^2$. The contribution due to F_L and the light flavors are not included. Statistical and full errors, obtained by adding the statistical and experimental systematic error in quadrature are shown. The change in the

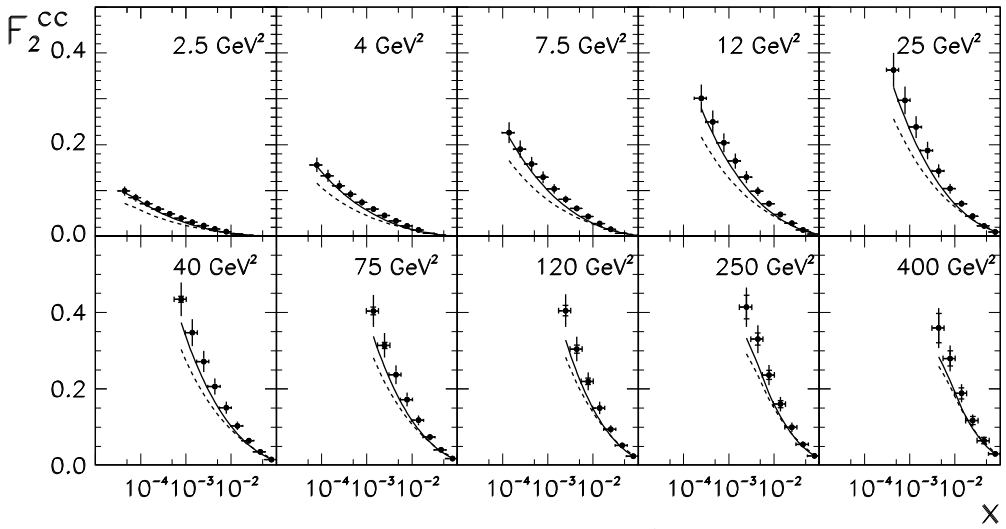

Figure 13: *Expected $F_2^{c\bar{c}}$ for a luminosity of 500 pb^{-1}. The points show the prediction from the gluon density determination by the NLO H1 fit to the inclusive F_2. The inner (outer) error represents the statistical and the total experimental error. The full (dashed) line gives the expectation from the NLO calculations based on GRV-HO and MRSH parton distributions using a charm quark mass of $m_c = 1.5$ GeV.*

acceptance due to the value of m_c and μ is not included in the error. For $Q^2 < 100$ GeV^2 the precision of this measurement will be limited by the experimental systematic uncertainty.

A detailed analysis of the experimental systematic uncertainties in the determination of $F_2^{c\bar{c}}$ with the current experimental statistics can be found in Ref. [1] for the H1 analysis. At present the total systematic error is approxiamtely 20 %. It is dominated by the uncertainty in the assumptions made to extract the signal from the observed mass distributions. This is clearly an effect of the limited statistics available in the current analyses. Because of the increase in statistical significance of the data with a luminosity of 500 pb^{-1} a much better understanding of the measured mass distributions as well as of the detector is expected. Ultimately a systematic error of 10% is achievable, which will then be to equal parts due to detector and analysis related errors (7%) and to the knowledge of the fragmentation probability $P(c \to D)$ of a charm quark into a specific charm meson and their branching ratios (7%). For the latter the experimental situation is not expected to improve in the near future.

Figure 13 also shows the NLO predictions using the GRV-HO(1992) and the MRSH parameterization of the gluon density in the proton using $m_c = 1.5$ GeV and $\mu^2 = Q^2 + 4m_c^2$. For a given value of m_c the data will still allow a sensitive indirect determination of the gluon density even with the relatively large experimental systematic uncertainties. Due to the high statistics it will be possible to measure the charm production cross section up to $Q^2 \geq 1000$ GeV^2. Assuming that charm tagging is performed for all decay modes listed in Tab. 4, the sensitivity limit for the inclusive measurements will already be reached at 50 pb^{-1} for $Q^2 \leq 100$ GeV^2, at which time the experimental systematic will dominate in this kinematic range.

The discussion in the theory section has shown, that the measurement of $F_2^{c\bar{c}}$ is sensitive to the gluon density to some extent at large y. Unfortunately the inclusive measurement in this range is also very sensitive on the charm quark mass. Therefore it is questionable whether the measurement of $F_2^{c\bar{c}}$ alone will allow an extraction of the gluon density at small x. In the experimental analysis of Ref. [1] it was observed that the change in $F_2^{c\bar{c}}$ at small Q^2 due to m_c is compensated by the change in the acceptance such that the measurement should still

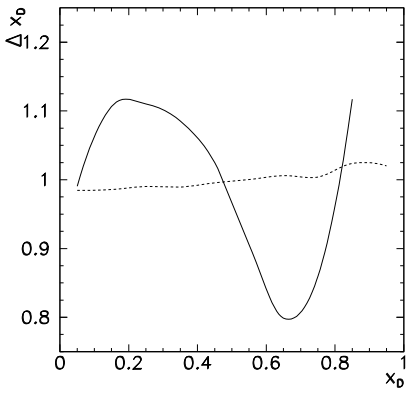

Figure 14: *Relative change Δx_D in the shape of the distribution $1/\sigma\ d\sigma/dx_D$ according to the LO Monte Carlo Simulation of the AROMA program for 6 $GeV^2 < Q^2 <$ 100 GeV^2 and the cuts of Eq. (11). The full line gives the change in the shape by changing m_c from 1.3 GeV to 1.7 GeV. The dashed line shows the influence of using the GRV-HO (1992) instead of the MRSH parameterization of the gluon density in the proton.*

allow the extraction of the gluon density from the inclusive measurement. The behavior of the acceptance at $Q^2 < 10$ GeV^2 has not been studied yet. If it happens that $F_2^{c\overline{c}}$ does not provide an reliable indirect extraction of the gluon density because of the uncertainty in m_c, exclusive distributions of the identified charm hadrons have to be studied. As an example the result of the Monte Carlo study of the influence of m_c and the gluon density on the distribution $1/\sigma\ d\sigma/dx_D$ is shown in Fig. 14 for 6 GeV$^2 < Q^2 <$ 100 GeV^2 and the cuts of Eq. (11). Here $\Delta\ x_D$ is defined as

$$\Delta\ x_D = \frac{1/\sigma_i\ d\sigma_i/dx_D(x_D)}{1/\sigma_j\ d\sigma_j/dx_D(x_D)} \tag{17}$$

where i, j denote the different values of the parameters, i.e. $m_c = 1.3,\ 1.7$ GeV and PDF=MRSH, GRV-HO(1992), respectively. The mass of the charm quark affects strongly the shape of the x_D distribution (full line) while there is only very little effect due to the choice of the parton density function (dashed line). A study of this distribution, for instance, should therefore disentangle the effect of the charm quark mass and the gluon density on $F_2^{c\overline{c}}$.

In section 2.5, the question when charm quarks should be treated as partons of the proton was discussed. The investigation of the x and Q^2 dependence of the exclusive measurement of $1/\sigma\ d\sigma/dx_D$ (see Fig. 11) will allow a study of the origin of charm production as a function of the kinematic variables. At sufficiently large Q^2 it is expected that the charm quark behaves like a parton in the proton. This will result in a change of the x_D distribution from the boson gluon fusion dominated regime presently observed in the available data at $\langle Q^2 \rangle \approx 25$ GeV^2 to the sea quark dominated regime at large Q^2. If it becomes possible to control the μ and m_c dependence of charm production at large Q^2, the measurement of $F_2^{c\overline{c}}(x, Q^2, x_D)$ can determine $g(x, Q^2)$ and $c(x, Q^2)$ simultaneously. This study would certainly require a luminosity of 500 pb^{-1} to produce enough data at large Q^2.

3.2.2 Bottom Production

In section 2.6, predictions for the number of bottom events as a function of x and Q^2 were given for a luminosity of 500 pb^{-1}. In the following the possibilities to measure $F_2^{b\overline{b}}(x, Q^2)$ at HERA will be discussed using again the H1 detector as an example.

Compared to charm quark events the major experimental difference in bottom quark production is the relatively long lifetime of the B mesons. With use of the CST, bottom events are selected by applying a cut in the impact parameter of tracks not fitting to the primary event vertex. The combinatorial background is negligible for this analysis, while the charm production is a significant background source, because of the much larger cross section. Two different possibilities will be discussed here, namely

1. the exclusive analysis of reconstructed D mesons. This method benefits from

   (a) the branching of B mesons into charm meson being very large [28], i.e. $BR(B \to D^{\pm}X) = 0.242 \pm 0.033$, $BR(B \to D^0/\overline{D}^0 X) = 0.58 \pm 0.05$ and $BR(B \to D^{*\pm})X = 0.0231 \pm 0.033$, and

   (b) the relatively long visible lifetime observed in these decay chains. Taking into account the decay length of both the B mesons and the subsequent D mesons, values of $c\tau \approx 590$ μm and $c\tau \approx 780$ μm are obtained for the decay chains $B \to D^0/\overline{D}^0 X$ and $B \to D^{\pm}X$, respectively. This has to be compared with the decay length the charm mesons of $c\tau = 124$ μm for the $D^0/\overline{D}^0$ and of $c\tau = 317$ μm for the $D^{\pm}$. Requiring a selection efficiency for the cut in the impact parameter of 50% would reduce the contamination of charm events by a factor of 12.5(2.8) in case of the $D^0(D^{\pm})$ analysis.

   All decay modes summarized in Tab. 4 will also be accessible in this case. Due to the larger cut values in the impact parameter for the different decay modes the combinatorial background is smaller. This will enable us to use softer cuts. Compared to the measurement of the charm production cross section in total an increase in efficiency by a factor 3 may be expected. A systematic error of 16% may be achieved. It will be dominated by the uncertainties in the branching fraction $BR(B \to DX)$.

2. the analysis of the impact parameter distribution of at least 3 to 4 tracks fitted to a common secondary vertex. Compared to the exclusive analysis this method leads to a higher selection efficiency, but will be limited by larger systematic uncertainties in the subtraction of the charm quark induced background.

Figure 15 shows the ratio of $F_2^{b\bar{b}}/F_2^{c\bar{c}}$ expected for the exclusive D meson analysis from bottom quark production using the the calculations of sections 2.1 and 2.6. The charm production background is subtracted statistically. The errors refer to the statistical and the total experimental error. For a luminosity of 500 pb^{-1} the error on the measurement of this ratio will still be statistics limited in most of the x and Q^2 plane. For a given Q^2 or x, this ratio is expected to rise with decreasing x or increasing Q^2, respectively. Integrated over the kinematic range a mean value of $F_2^{b\bar{b}}/F_2^{c\bar{c}} \approx 0.02$ is predicted.

4 Conclusions

In this paper, we have discussed DIS heavy-flavour production at HERA at NLO. The effect on the charm production cross section due to the uncertainties in the factorization/renormalization scale μ and the charm quark mass m_c has been studied as a function of x and Q^2. At small

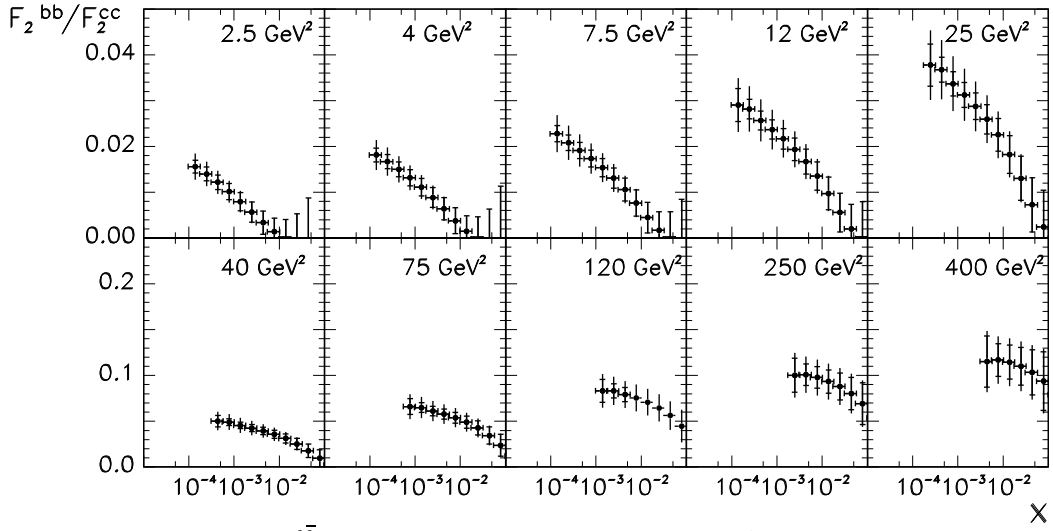

Figure 15: *Expected ratio $F_2^{b\bar{b}}/F_2^{c\bar{c}}$ for a luminosity of 500 pb^{-1}. The points show the predictions according to the calculations of section 2.1 and 2.6. The inner (outer) error represents the statistical and the total experimental error.*

x and for $Q^2 < 300$ GeV^2 the predictions are found to be insensitive to μ while in this region the effect of m_c is found to be large. Unfortunately the sensitivity of $F_2^{c\bar{c}}(x, Q^2)$ to the gluon density is also restricted to this kinematic region. It has been shown that the contribution of F_L has sizeable effects on the charm production cross section at large y. The contribution of light quarks to the cross section turned out to be of the order of 5%, nearly independent of x and Q^2. Results on bottom production have been presented.

The current experimental situation has been summarized. Based upon this knowledge, statistical and experimental systematic uncertainties for large luminosity have been estimated. Ultimately an accuracy of 10% in the overall normalization of the cross section may be achieved. In the kinematic range where the inclusive measurement $F_2^{c\bar{c}}(x, Q^2)$ is found to be sensitive to the gluon density, the error of the inclusive measurement will start to be systematics dominated with a luminosity of 50 pb^{-1}. It has been demonstrated that exclusive measurements of the charm mesons would disentangle the influence of m_c and the gluon density on the charm production cross section. An exploration of the kinematic plane, the extraction of the gluon density, as well as the question when the charm quark may be treated as a parton, will require a luminosity of 500 pb^{-1}. Finally the ratio of $F_2^{b\bar{b}}/F_2^{c\bar{c}}(x, Q^2)$ has been investigated by performing an exclusive D meson analysis. With a luminosity of 500 pb^{-1} the predicted statistics is found to be sufficient to make a detailed study of the x and Q^2 dependence of this ratio.

Acknowledgments

S.R. thanks Jenny Ivarsson for her help making the figures and Fred Jegerlehner for reading the manuscript.

References

[1] C. Adloff *et al.*, H1 Collaboration, DESY 96-138, accepted by Z. Phys. **C** (1996).

[2] ZEUS Collaboration, contributed paper to XXVIII Int. Conf. on HEP '96, Warsaw (1996).

[3] E. Laenen, S. Riemersma, J. Smith, and W.L. van Neerven, Nucl. Phys. **B392** (1993) 162.

[4] E. Laenen, S. Riemersma, J. Smith, and W.L. van Neerven, Nucl. Phys. **B392** (1993) 229.

[5] B.W. Harris and J. Smith, Nucl. Phys. **B452** (1995) 109; Phys. Lett. **353B** (1995) 535; B.W. Harris, talk A05057, presented at the American Physical Society, Division of Particles and Fields 1996 Meeting, Minneapolis, Minnesota, 10-15 August 1996, to appear in proceedings.

[6] M. Buza, Y. Matiounine, R. Migneron, J. Smith, and W.L. van Neerven, Nucl. Phys. **B472** (1996) 611.

[7] S. Riemersma, J. Smith, and W.L. van Neerven, Phys. Lett. **347B** (1995) 143.

[8] E. Laenen, S. Riemersma, J. Smith, and W.L. van Neerven, Phys. Letts. **291B** (1992) 325.

[9] A. Vogt, DESY 96-012, hep-ph/9601352

[10] E. Laenen, M. Buza, B.W. Harris, Y. Matiounine, R. Migneron, S. Riemersma, J. Smith, and W.L. van Neerven, these proceedings.

[11] Handbook of Mathematical Functions, eds. M. Abramowitz and I.E. Stegun, National Bureau of Standards, (1972) 879.

[12] H.L. Lai, J. Botts, J. Huston, J.G. Morfin, J.F. Owen, J.W. Qiu, W.K. Tung, and H. Weerts, Phys. Rev. **D51** (1995) 4763.

[13] M. Glück, E. Reya, and A. Vogt, Z. Phys. **C67** (1995) 433.

[14] M.A.G. Aivazis, F.I. Olness, and W-K. Tung, Phys. Rev. **D50** (1994) 3085; M.A.G. Aivazis, J.C. Collins, F.I. Olness, and W-K. Tung, Phys. Rev. **D50** (1994) 3102.

[15] M. Buza, Y. Matiounine, J. Smith and W.L. van Neerven, in preparation.

[16] G. Feldmann *et al.*: Phys. Rev. Lett. **38** (1977) 1313.

[17] S. Aid et al., H1 Coll.: Nucl. Phys. **B470** (1996) 3.

[18] G. Ingelman, J. Rathsman, and G.A. Schuler: DESY preprint, DESY 96-058, and hep-ph/9605285.

[19] T. Sjöstrand: "PYTHIA 5.7 and JETSET 7.4 Physics and Manual", CERN-TH.7112/93.

[20] G. Ingelman: "LEPTO version 6.1 - The Lund Monte Carlo for Deep Inelastic Lepton-Nucleon Scattering", TSL/ISV-92-0065.

[21] H. Abramowicz et al., CDHS Coll.: Z. Phys. **C15** (1982) 19; N. Ushida et al., E531 Coll.: Phys. Lett. **206B** (1988) 380.

[22] J.J. Aubert et al., EMC Coll.: Nucl. Phys. **B213** (1983) 31.

[23] M. Glück, E. Reya, and A. Vogt, Z. Phys. **C53** (1992) 127.

[24] P.N. Harriman, A.D. Martin, W.J. Stirling, and R.G. Roberts, Phys.Rev.**D42** (1990) 798.

[25] A.D. Martin, R.G. Roberts, and W.J. Stirling, Phys. Lett. **306B** (1993) 145.

[26] S. Aid et al., H1-Coll, DESY 96-01, accepted to Nucl. Inst. and Meth. (1996).

[27] W. Erdmann et al., Nucl. Inst. and Meth. **A372** (1996) 188.

[28] R.M. Barnett et al., Particle Data Group, Phys. Rev. **D54** (1996) 1.